

UpCycling: Semi-supervised 3D Object Detection without Sharing Raw-level Unlabeled Scenes

Sunwook Hwang[†] Youngseok Kim[†] Seongwon Kim[§] Saewoong Bahk[†] * Hyung-Sin Kim[‡] *

[†]Department of Electrical and Computer Engineering, Seoul National University, *Corresponding author

[§]Multimodal AI in SK Telecom, Seoul, Korea, [‡]Graduate School of Data Science, Seoul National University

{swhwang, yskim}@netlab.snu.ac.kr, slkim@sktbrain.com, {sbahk, hyungkim}@snu.ac.kr

Abstract

Semi-supervised Learning (SSL) has received increasing attention in autonomous driving to relieve enormous burden for 3D annotation. In this paper, we propose UpCycling, a novel SSL framework for 3D object detection with zero additional raw-level point cloud: learning from unlabeled de-identified intermediate features (i.e., smashed data) for privacy preservation. The intermediate features do not require additional computation on autonomous vehicles since they are naturally produced by the inference pipeline. However, augmenting 3D scenes at a feature level turns out to be a critical issue: applying the augmentation methods in the latest semi-supervised 3D object detectors distorts intermediate features, which causes the pseudo-labels to suffer from significant noise. To solve the distortion problem while achieving highly effective SSL, we introduce hybrid pseudo labels, feature-level Ground Truth sampling (F-GT) and Rotation (F-RoT), which safely augment unlabeled multi-type 3D scene features and provide high-quality supervision. We implement UpCycling on two representative 3D object detection models, SECOND-IoU and PV-RCNN, and perform experiments on widely-used datasets (Waymo, KITTI, and Lyft). While preserving privacy with zero raw-point scene, UpCycling significantly outperforms the state-of-the-art SSL methods that utilize raw-point scenes, in both domain adaptation and partial-label scenarios.

1. Introduction

Although the concept of Autonomous Vehicles (AVs) has been around for years, ensuring the safety of users driving AVs on real roads via 3D object detection models is still challenging. To this end, there have been continuous efforts to collect large datasets of 3D road scenes and annotate them carefully [8, 11, 32]. While rapid advances in sensor technology facilitate the collection of 3D scenes at scale, the severe *annotation burden* remains as a main challenge. To alleviate the problem, a couple of semi-supervised learning (SSL) methods for 3D object detection have been proposed

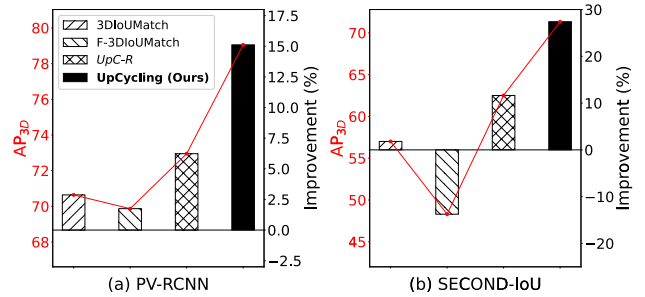


Figure 1. Performance of SSL for 3D object detection on a partial-label scenario (Section 4.3) where 10% data are labeled in the KITTI dataset and test difficulty is Moderate. Horizontal lines represent performance of the baseline using only the labeled data.

recently, such as a combination of perturbation and consistency loss [44] and confidence-based filtering using IoU prediction results [38]. However, these methods learn from unlabeled raw 3D scenes. Collecting a vast amount of raw-level road scenes from AVs can potentially cause disclosure of sensitive private information on the roads [7, 21, 41].

Given that the problem of potential *privacy leakage* from raw data collection exists in various applications, a number of studies have tried to not deal with raw data directly. Going beyond encrypting raw data [41], federated learning [9, 13] makes each edge node consume its data locally to train the model and share the model weights (or gradients) instead of raw data. Split learning [9, 30, 35] designs edge nodes to not share raw data but its intermediate feature (i.e., smashed data) that comes from passing through early-stage layers of the model. However, these approaches require local training [26, 29], which makes resource-constrained AVs suffer more *computation overhead*. Given that AVs use significant computing resources to process inference pipelines for 3D detection during driving, such additional computation hinders continuous model updates in natural driving conditions.

In this paper, we aim to address all the three issues: labeling cost, privacy, and AV-side computation overhead. To ensure this end, we propose UpCycling, a novel SSL framework that does not utilize unlabeled raw 3D scenes but *de-identified, unlabeled* intermediate features to advance 3D

object detection models. Since an unlabeled intermediate feature is naturally produced during a regular detection pipeline with the 3D scene, UpCycling requires neither additional AV-side computation (*e.g.*, local training) nor server-side annotation burden. Further, sharing features instead of raw 3D scenes improves the level of privacy protection as the detection pipeline includes nonlinear layers and compression [5, 16, 27, 42, 45]. Because the process in the nonlinear layers [36] is irreversible, the original scene cannot be completely restored from its intermediate feature.

To realize the advantages, UpCycling should provide an effective feature-based SSL method for 3D object detection, which involves two challenges: (1) augmenting unlabeled intermediate features reliably to increase data diversity [12, 15] and (2) providing high-quality pseudo labels to supervise these augmented features. It is difficult to apply the augmentation methods used for the state-of-the-art (SOTA) semi-supervised 3D object detection [38, 44] since they target raw-level point clouds. In contrast, an intermediate feature is a smashed form of its original 3D scene and has multiple types depending on the 3D object detection models, such as grid- and set-types. Therefore, naïve application of the point augmentation methods at a feature level damages the important information in the 3D scene, which causes the pseudo labels to suffer from significant noise. As shown in Figure 1, the latest 3DIoUMatch [38] experiences performance degradation when applied at a feature level (*i.e.*, 3DIoUMatch vs. F-3DIoUMatch) and becomes even worse than the baseline that relies only on limited labeled data (Figure 1(b)).

To address the challenges, we propose high-quality *hybrid pseudo labels*, feature-level ground-truth sampling (*F-GT*), and feature-level rotation (*F-RoT*). Combining the three not only achieves significant data diversity but also improves quality of pseudo labels by adding zero-noise labels. We implement UpCycling on two representative 3D detection models, PV-RCNN [27] and SECOND-IoU [34],¹ and perform various experiments on three major datasets for AV applications, KITTI [8], Lyft [11], and Waymo [32]. The results demonstrate the effectiveness of UpCycling in both partial-label and domain adaptation scenarios.

Interestingly, while preserving privacy, UpCycling significantly outperforms the SOTA SSL methods that utilize raw-level scenes [38, 43]. For example, in a partial-label scenario (Figure 1), UpCycling improves accuracy over 3DIoUMatch by 11.9% on PV-RCNN and 25.1% on SECOND-IoU. In addition, UpCycling performs better than its ablated version (*UpC-R*) that utilizes raw-point scenes. Although our motivation was privacy protection, the experimental results suggest rethinking the unlabeled feature-based learning, as an effective way of accuracy improvement for semi-supervised 3D object detection.

¹SECOND-IoU adds an IoU module to the original SECOND model [42].

The contributions of this work are summarized as follows:

- UpCycling is the first framework that tackles labeling cost, privacy leakage, and AV-side computation cost altogether to train a 3D object detection model, which deeply investigates how to learn from unlabeled intermediate features.
- *F-GT* provides a fresh eye on GT sampling in the context of SSL since it significantly improves pseudo-label quality by providing zero-noise labels. *F-RoT* reveals that rotation at a feature level provides additional strong diversity effect. *F-GT* and *F-RoT* create synergy to boost performance.
- Without using unlabeled raw 3D scenes, UpCycling achieves SOTA accuracy with large margins in both domain adaptation and partial-label scenarios, on representative models and datasets for 3D object detection.

2. Related Work

Semi-supervised learning. SSL has been actively studied in the context of image classification [15, 22, 31, 33]. Most of the recent SSL methods [12, 15, 22, 33] leverage consistency regularization which trains the model to obtain consistent prediction results across label-preserving data augmentation. In the SSL frameworks, proper data augmentation is essential, which should significantly increase diversity effect without losing consistency with the original data [4, 6]. Accurate pseudo-labeling is another crucial element for SSL to provide high-quality supervision for unlabeled data [17, 31]. While there have been only a couple of studies on SSL for 3D object detection [38, 44], data augmentation and pseudo-labeling are still important. SESS [44] targets indoor 3D object detection, leveraging a teacher-student architecture that takes differently augmented 3D scenes as inputs and utilizes three kinds of consistency losses between outputs. 3DIoUMatch [38] improves quality of pseudo labels with confidence-based filtering in the IoU-guided NMS stage. However, the SSL methods require direct access to a vast amount of raw data, which causes potential privacy leakage.

Feature-level data augmentation. While there exist powerful augmentation tools [4, 6], data diversity can still be limited when augmenting only raw data. To further increase diversity, feature-level data augmentation has been investigated [2, 3, 18, 19, 37]. In image classification tasks, adding Gaussian noise to feature-level data gains more data diversity for training and domain generalization [18]. The work in [2, 3, 19] resolves lack of data for specific classes by using feature augmentation. Feature augmentation is also applied to few-shot learning in NLP tasks [14]. To our knowledge, however, feature-level augmentation has not been studied in the context of semi-supervised 3D object detection.

Private representation learning. Private representation learning [9, 13] aims to learn from various clients without sharing their raw data, which heavily relies on local training at resource-constrained clients. Federated learning designs

pipeline. Each AV also sends the detection results $\{\tilde{\mathbf{y}}^u\}$ to the server.

With the received features and detection results $\{\mathbf{f}_i^u, \{\tilde{\mathbf{y}}_i^u\}_{i=1}^{N^u}\}$, the server enforces consistency regularization for effective training, in a different way of the SOTA SSL methods on 3D object detection that utilize unlabeled raw-point scenes $\{\mathbf{x}_i^u\}_{i=1}^{N^u}$ [38, 44]. Specifically, given that supervising \mathbf{f}^u by using its detection result $\{\tilde{\mathbf{y}}^u\}$ again is meaningless, (1) proper augmentation of \mathbf{f}^u and (2) high-quality pseudo labels are essential for the success of UpCycling.

The SOTA methods on semi-supervised 3D object detection [38, 44] take a teacher-student architecture [33], which heavily relies on the two assumptions: (1) strongly and weakly augmented versions of a 3D point cloud scene are different but correlated enough to share the same pseudo labels, (2) the teacher network is in a position of advantage by taking the weakly augmented scene, which produces pseudo labels accurate enough to supervise the strongly augmented scene. The work in [44] found that both assumptions hold when using random sampling (RS) for weak augmentation and both RS and Flip for strong augmentation. However, in our scenario where an input is an intermediate feature, the augmentation methods do not satisfy the two requirements.

Instead, we propose feature-level ground-truth sampling (*F-GT*) and Rotation (*F-RoT*) for feature augmentation, as illustrated in Figure 2. Although ground-truth (GT) sampling has been used as a data augmentation method for supervised 3D object detection [5, 16, 27, 42, 45] and is known to provide at most fair performance improvement [10], we claim that its impact can be more significant when it comes to feature-level augmentation of an unlabeled scene. This is because *F-GT* tackles one of the most crucial issues for successful SSL: improving the quality of pseudo labels for unlabeled features by generating *hybrid pseudo labels*. In addition, *F-RoT* perturbs a scene feature significantly enough to gain *additional diversity effect* even when Rotation is already applied for augmenting the raw-point scene.

3.3. Hybrid Pseudo Labels

Generating high-quality pseudo labels for an unlabeled feature-level scene is necessary for effective SSL. To this end, we adopt *F-GT* to augment an unlabeled scene feature \mathbf{f}^u and include the sampled GT labels in the pseudo-label set for the unlabeled feature, resulting in high-quality *hybrid pseudo labels*.

Confidence-based pseudo-label filtering. First, inspired by 3DIoUMatch [38], UpCycling screens the received detection results $\{\tilde{\mathbf{y}}^u\}$ by using each $\tilde{\mathbf{y}}^u$'s confidence scores for both object classification and bounding box localization. Assume that τ_{IoU} and τ_{cls} are thresholds for box localization and object classification, respectively. UpCycling filters out a detection result if its class confidence or localization confidence is lower than the given threshold, leaving

a set of high-quality pseudo labels, denoted as $\{\hat{\mathbf{y}}^u\}$. The confidence-based pseudo-label filtering is applied for more accurate supervision.

Pseudo-label-aware GT sampling. When GT sampling is applied for supervised learning, it first constructs a GT database that consists of labeled 3D bounding boxes and point clouds in the boxes, collected from the entire labeled training set $\{\mathbf{x}_i^l, \{\mathbf{y}_i^l\}_{i=1}^{N^l}\}$. To augment a labeled 3D scene \mathbf{x}^l , GTs are sampled from the database and randomly placed in the 3D scene. To avoid tampering with GT information, a GT sample that overlaps with a ground-truth bounding box in the original labeled scene is removed.

In contrast, our *F-GT* aims to augment an *unlabeled* 3D scene feature \mathbf{f}^u without accurate box labels. Instead, given that a set of high-quality pseudo labels $\{\hat{\mathbf{y}}^u\}$ is provided, *F-GT* samples GTs that do not overlap with the *pseudo labels*. Importantly, although the pseudo labels are filtered with the two thresholds τ_{IoU} and τ_{cls} , these thresholds are set moderately [38], enabling the pseudo labels to cover most objects in the original scene \mathbf{x}^u ; GT samples are likely to be placed on the background of \mathbf{x}^u .

Hybrid pseudo labels. To generate pseudo labels that supervise an augmented unlabeled feature \mathbf{f}_{aug}^u , UpCycling merges the high-quality pseudo-label set for the original feature \mathbf{f}^u , $\{\hat{\mathbf{y}}^u\}$, with the label set for the GT samples, $\{\mathbf{y}^{GT}\}$, resulting in a set of *hybrid pseudo labels* $\{\hat{\mathbf{y}}^u\} \cup \{\mathbf{y}^{GT}\}$. Given that $\{\mathbf{y}^{GT}\}$ are literally ground-truth labels with *zero noise*, adding these labels to the pseudo labels enables powerful supervision. Furthermore, generating the hybrid pseudo labels does not need to execute the inference pipeline at the server, since all GT labels are already given.

3.4. Feature-level 3D Scene Augmentation

UpCycling executes *F-GT* and *F-RoT* sequentially to augment a 3D point cloud scene at a feature level, resulting in \mathbf{f}_{aug}^u . Regarding *F-GT*, since the server does not have an original unlabeled scene \mathbf{x}^u but only its intermediate feature \mathbf{f}^u , it is impossible to directly place GT samples on the point cloud scene. Instead, *F-GT* generates a separate point cloud input that comprises only GT samples. The GT-only point cloud passes through the model's 3D backbone network, resulting in a GT-only feature \mathbf{f}^{GT} . Note that while the 3D backbone of SECOND-IoU generates only grid-type features, that of PV-RCNN [27] generates both grid- and set-type features. To this end, *F-GT* and *F-RoT* augment \mathbf{f}^u , grid- or set-type feature, as follow:

Grid-type feature augmentation. As shown in Figure 2, when \mathbf{f}^u and \mathbf{f}^{GT} are grid-type features, *F-GT* generates a weakly augmented feature by overwriting \mathbf{f}^u with \mathbf{f}^{GT} ; if a channel on \mathbf{f}^{GT} has non-zero values, the \mathbf{f}^{GT} channel replaces that in \mathbf{f}^u . Giving higher priority for \mathbf{f}^{GT} removes some information included in \mathbf{f}^u . However, given that the

GT samples take up a tiny portion of an entire scene (*i.e.*, most values in \mathbf{f}^{GT} are zero), only a small number of values in \mathbf{f}^u are modified. In addition, the removed information in \mathbf{f}^u is related to the background since the sampled GTs are not overlapped with pseudo labels, which does not harm model training. Lastly, *F-RoT* rotates the weakly augmented feature with a degree randomly selected from $[-45^\circ, 45^\circ]$ and performs bilinear interpolation to compensate for errors, resulting in the final strongly augmented feature \mathbf{f}_{aug}^u .

Set-type feature augmentation. When an unlabeled feature \mathbf{f}^u and a GT sample feature \mathbf{f}^{GT} are set types, each of them consists of n represented points, denoted as $\mathbf{f}^u = \{\mathbf{f}_i^u\}_{i=1}^n$ and $\mathbf{f}^{GT} = \{\mathbf{f}_i^{GT}\}_{i=1}^n$, respectively. In this case, as illustrated in Figure 2, *F-GT* generates a weakly augmented feature as a point set, denoted as $\mathbf{f}_{aug}^u = \{\mathbf{f}_{aug,i}^u\}_{i=1}^n$. To this end, we first exclude the scene feature points \mathbf{f}_i^u that are in the GT boxes, generating $\mathbf{f}^{u \setminus GT}$. Then each feature point $\mathbf{f}_{aug,i}^u$ is randomly sampled from either $\mathbf{f}^{u \setminus GT}$ or \mathbf{f}^{GT} .

In doing so, it is important that the scene feature contains much more information than the GT feature; for reasonable augmentation, \mathbf{f}_{aug}^u should include scene feature points more than GT feature points. To determine proper sampling frequency, we utilize the information in the grid-type feature that is generated simultaneously with the set-type feature by the 3D backbone network: how many values in the grid-type feature for the scene and GT samples are non-zero. For example, if the number of grid with non-zero values in the scene and GT features (grid types) is 2000 and 50, respectively, points in the augmented feature set \mathbf{f}_{aug}^u is sampled from $\mathbf{f}^{u \setminus GT}$ 400 times more than \mathbf{f}^{GT} . Lastly, *F-RoT* further perturbs the weakly augmented feature \mathbf{f}_{aug}^u by rotating it with a degree randomly selected from $[-45^\circ, 45^\circ]$.

3.5. Loss

The model’s detection head is trained to predict the hybrid pseudo labels for the strongly augmented feature \mathbf{f}_{aug}^u . This enforces consistency regularization because the strongly augmented scene is significantly different from the weakly augmented scene that matches the hybrid pseudo labels. Given that our target models have an IoU module as well as a Region Proposal Network (RPN), the unlabeled loss $\mathcal{L}(\mathbf{f}_{aug}^u)$ includes loss of each of the two modules as follows:

$$\begin{aligned} \mathcal{L}(\mathbf{f}_{aug}^u) = & \mathcal{L}_{loc}^{RPN}(\{\hat{\mathbf{y}}^u\} \cup \{\mathbf{y}^{GT}\}) + \mathcal{L}_{loc}^{IoU}(\{\hat{\mathbf{y}}^u\} \cup \{\mathbf{y}^{GT}\}) \\ & + \mathcal{L}_{cls}^{RPN}(\{\hat{\mathbf{y}}^u\} \cup \{\mathbf{y}^{GT}\}). \end{aligned} \quad (1)$$

The exact calculation of the three terms depends on the model architecture, following the calculation of supervised loss. Assuming that a training batch consists of a set of labeled scenes $\{\mathbf{x}^l\}$ and a set of augmented features for unlabeled scenes $\{\mathbf{f}_{aug}^u\}$, the total loss for the batch is calculated as below, where w is the unsupervised loss weight:

$$\mathcal{L}_{total} = \mathcal{L}(\{\mathbf{x}^l\}) + w\mathcal{L}(\{\mathbf{f}_{aug}^u\}). \quad (2)$$

Table 1. Results of domain adaptation tasks when Waymo is the source dataset and Lyft and KITTI are target datasets. Difficulty of the KITTI test dataset is set as Moderate. **Top-1 values** and **2nd best values** are indicated in each case.

Dataset	Method	SECOND-IoU	PV-RCNN
		AP _{BEV} / AP _{3D}	AP _{BEV} / AP _{3D}
Lyft	Baseline	30.20 / 21.32	33.00 / 24.49
	SN	28.38 / 19.25	33.44 / 25.64
	ST3D	60.53 / 29.90	62.28 / 42.63
	ST3D (w/ SN)	52.86 / 21.25	60.15 / 44.02
	<i>F-GT</i>	68.83 / 45.66	63.38 / 46.83
	<i>F-GT</i> (w/ SN)	65.10 / 49.24	63.58 / 49.35
	UpCycling	69.62 / 53.80	66.27 / 53.59
	UpCycling (w/ SN)	69.11 / 53.17	64.93 / 52.67
	Oracle	76.70 / 61.70	78.68 / 64.54
KITTI	Baseline	54.14 / 10.16	62.24 / 9.24
	SN	60.80 / 37.30	60.08 / 38.86
	ST3D	70.90 / 40.16	66.19 / 23.26
	ST3D (w/ SN)	80.97 / 57.68	54.30 / 48.79
	<i>F-GT</i>	58.26 / 11.71	62.09 / 11.35
	<i>F-GT</i> (w/ SN)	80.30 / 51.03	85.90 / 61.12
	UpCycling	78.62 / 59.16	85.93 / 77.54
	UpCycling (w/ SN)	84.56 / 75.05	86.69 / 81.17
	Oracle	90.36 / 82.02	90.84 / 84.56

4. Experiments

4.1. Experimental Setup

Scenarios. To demonstrate the effectiveness of UpCycling in various practical situations, we conduct experiments in both domain adaptation and partial-label scenarios. The domain adaptation task is to adapt the model, which is trained on abundant labeled data in the source domain, to an unseen target domain that provides only unlabeled data. In the partial-label scenario, the model is trained and tested in the same domain but most of the training data is unlabeled.

Datasets. We choose three datasets widely used for detection applications of AVs: Waymo [32], Lyft [11], and KITTI [8]. Among the three, the Waymo dataset is the most diverse and the largest in volume. The 3D scenes in the Waymo dataset are captured in Phoenix, Mountain View, and San Francisco, the US, under multiple weather and time settings. The Lyft dataset is collected around Palo Alto, the US, in clear weather in the daytime. The KITTI dataset is collected in Karlsruhe, Germany, in clear weather during the daytime. Due to regional characteristics, car sizes in KITTI are different from those in Waymo and Lyft [40]. More detailed information is indicated in the supplementary material.

Implementation details. When training a model with UpCycling, we set the two filtering thresholds τ_{IoU} and τ_{cls} to 0.5 and 0.4, respectively, and the weight for the loss $\mathcal{L}(\{\mathbf{f}_{aug}^u\})$ is set as $w = 1$. We set the ratio of labeled data to unlabeled data in a mini-batch to 1:2 and 1:1 for do-

Table 2. Results of partial-label scenarios with three different ratios of labeled data in the KITTI dataset: 2%, 10%, 25%. **Top-1 values** and **2nd best values** are indicated in each case.

AP _{3D}		2%			10%			25%		
SECOND-IoU	Baseline	56.69	44.11	37.19	70.58	56.00	47.94	84.47	71.06	62.87
	3DIoUMatch	63.57	49.58	43.00	71.76	57.01	50.08	81.71	68.51	60.92
	<i>F-GT</i>	70.19	59.97	44.83	76.09	60.41	51.84	85.22	72.87	63.93
	UpCycling	81.98	68.99	63.88	84.05	71.34	64.36	87.12	76.20	70.27
	Improved (%)	44.61	56.41	71.77	19.08	27.4	34.25	3.14	7.24	11.77
PV-RCNN	Baseline	68.10	53.27	46.20	81.23	68.67	60.32	87.63	76.03	68.62
	3DIoUMatch	81.04	65.77	58.83	85.26	70.64	63.32	85.08	72.37	65.02
	<i>F-GT</i>	76.46	61.44	52.94	83.64	69.60	63.53	88.05	76.61	70.80
	UpCycling	88.07	75.97	70.74	90.17	79.05	75.19	90.50	82.02	76.98
	Improved (%)	29.32	42.6	53.12	11.00	15.11	24.66	3.27	7.88	12.19

main adaptation and partial-label experiments, respectively. Importantly, *F-GT* samples GT boxes only from the labeled dataset: the source domain data in the domain adaptation scenario and a small portion of labeled data in the partial-label scenario. Lastly, UpCycling freezes the 3D backbone network after training it on the labeled data to prevent the divergence between an intermediate feature from the server’s 3D backbone network and that collected from AVs. Therefore, UpCycling updates only the detection head using unlabeled feature-level data. More details are in the supplementary material.

4.2. Domain Adaptation Experiments

In domain adaptation experiments, we use the Waymo dataset as the source domain and the Lyft and KITTI datasets as the target domains. The model is first pre-trained on the source domain’s labeled data (called the baseline model), adapted using unlabeled training data in a target domain, and then tested on the target domain’s test data.

Comparison schemes. We compare UpCycling with various methods. **Baseline** evaluates the baseline model directly and **Oracle** adapts the model with fully supervised learning in the target domain, which provide the lower- and upper-bound performance, respectively. **ST3D** [43] and **SN** (Statistical Normalization) [40] are the SOTA domain adaptation methods on 3D object detection that utilize unlabeled raw 3D scenes. ST3D generates pseudo labels from unlabeled data in the target domain to adapt the baseline model. SN assumes that statistical object sizes in the target domain are given and trains the baseline model in the source domain using the target domain object size information. *F-GT* is an ablated UpCycling that excludes strong augmentation (*F-RoT*). We also evaluate variants of ST3D, *F-GT* and our UpCycling by combining SN together, denoted as (**w/ SN**).

Result analysis. Table 1 shows the results of UpCycling and the various comparison methods on SECOND-IoU and PV-RCNN. The results show that although UpCycling (or w/ SN) does not utilize raw-point scenes for privacy protection, it *always provides the best accuracy* regardless of the

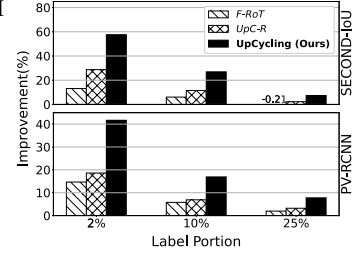


Figure 3. Effects of hybrid pseudo label and feature-level augmentation in partial-label scenarios, showing the average performance improvement over Baseline in all KITTI test cases.

model, dataset, and detection task (BEV or 3D). Specifically, UpCycling significantly outperforms the two SOTA methods (ST3D and SN). When compared to the better option between ST3D (or w/ SN) and SN in each case, UpCycling improves accuracy by **3.59~20.5** AP_{BEV} and **9.57~32.38** AP_{3D}. The results demonstrate the effectiveness of hybrid pseudo labels and feature-level augmentation schemes in UpCycling and also suggest the potential of using unlabeled features to advance 3D object detection models.

Taking a deeper look, UpCycling outperforms and underperforms UpCycling (w/ SN) in the Lyft and KITTI datasets, respectively. Given that Waymo and Lyft are collected from the US but KITTI is collected from Germany, object sizes in KITTI are different from those in Lyft and Waymo. Since SN adjusts object sizes, applying SN clearly improves accuracy of UpCycling in KITTI but not in Lyft. Lastly, UpCycling improves accuracy over *F-GT* in most cases, verifying that gaining additional data diversity using *F-RoT* boosts the effect of consistency regularization.

4.3. Partial-label Experiments

In partial-label experiments, we train SECOND-IoU and PV-RCNN on the KITTI dataset when only a small portion of its training data is labeled. Importantly, given that the KITTI dataset is originally shuffled regardless of place and time sequence, we rearrange it in chronological order for each place to prevent the data leakage between the labeled and unlabeled sets [1].

Comparison schemes. In this scenario, **Baseline** trains the model using only the limited amount of labeled data. **3DIoUMatch** [38] is the SOTA SSL method using unlabeled raw-point scenes. For consistency regularization, 3DIoUMatch uses Flip and RS to augment raw data and filters pseudo labels in the IoU-guided NMS.² As in Section 4.2, *F-GT* excludes *F-RoT* from UpCycling.

²Since the authors in [38] did not use the rearranged KITTI dataset in their experiments, we measure the performance of 3DIoUMatch again in the rearranged KITTI dataset. In addition, we newly implement 3DIoUMatch on SECOND-IoU for more extensive comparison.

Table 3. Effects of hybrid pseudo label and feature-level augmentation in the domain adaptation scenarios with the same settings as Table 1. HPL and FA indicate hybrid pseudo label and feature-level augmentation, respectively.

Dataset	Method	HPL	FA	AP_{3D} (Closed Gap[%])	
				SECOND-IoU	PV-RCNN
KITTI	Baseline	-	-	10.16 (0.00)	9.24 (0.00)
	<i>UpC-R</i> (w/ SN)	✓	-	53.05 (59.69)	52.99 (58.09)
	<i>F-RoT</i> (w/ SN)	-	✓	44.25 (47.44)	44.56 (46.90)
	UpCycling (w/ SN)	✓	✓	75.05 (90.31)	81.17 (95.49)
	Oracle	-	-	82.02 (100.0)	84.56 (100.0)
Lyft	Baseline	-	-	21.32 (0.00)	24.49 (0.00)
	<i>UpC-R</i>	✓	-	46.30 (61.86)	48.96 (61.10)
	<i>F-RoT</i>	-	✓	46.37 (62.04)	47.90 (58.46)
	UpCycling	✓	✓	53.80 (80.45)	53.59 (72.66)
	Oracle	-	-	61.70 (100.0)	64.54 (100.0)

Table 4. Effects of feature-level augmentation methods in the partial-label scenarios with the same settings as Table 2. The 3D object detection model is SECOND-IoU and 10% training data is labeled in KITTI. Policy 4* indicates F-3DIoUMatch in Figure 1.

Policy #	Flip	Noise	RS	F-GT	F-RoT	AP_{3D}		
						Easy	Mod	Hard
Baseline	-	-	-	-	-	70.58	56.00	47.94
1	✓	-	-	-	-	-16.31	-20.09	-19.79
2	-	✓	-	-	-	+0.03	+0.13	-1.23
3	-	-	✓	-	-	+2.47	-0.96	+0.63
4*	✓	-	✓	-	-	-11.69	-13.75	-13.32
5	-	-	-	✓	-	+4.80	+5.42	+7.96
6	-	-	-	-	✓	+7.81	+7.87	+8.14
UpCycling	-	-	-	✓	✓	+13.47	+15.34	+16.42

Result analysis. As shown in Table 2, UpCycling achieves the best accuracy in all cases with large margins, regardless of the ratio of labeled data, model, and task difficulty. Without having access to unlabeled raw data, UpCycling provides much better performance compared to 3DIoUMatch. For example, with 2% labeled data, UpCycling improves accuracy over 3DIoUMatch **18.41~20.88** AP_{3D} on SECOND-IoU and **7.03~11.91** AP_{3D} on PV-RCNN. Interestingly, even the ablated version *F-GT* outperforms 3DIoUMatch in most cases, which demonstrates the effectiveness of adding zero-noise labels to pseudo labels for powerful supervision. Lastly, it is important to note that naïve application of 3DIoUMatch at a feature level degrades performance, as shown in Figure 1 (F-3DIoUMatch); remarkable performance improvement of UpCycling comes from its tailored design to handle feature-level 3D scenes.

4.4. Ablation Studies

Effect of each component. We evaluate the effect of two main components in UpCycling, hybrid pseudo label and feature augmentation, by using two comparison schemes *UpC-R* and *F-RoT*. *UpC-R* is the application of UpCycling at the raw-level input, meaning that both GT sampling and Rotation augment a raw-point scene instead of its feature. Thus, *UpC-R* excludes feature augmentation from UpCycling but still contains hybrid pseudo label. *F-RoT* excludes *F-GT*

from UpCycling, which preserves strong feature-level augmentation but removes hybrid pseudo labels.

Figure 3 compares UpCycling with *UpC-R* and *F-RoT* in the partial-label scenario described in Section 4.3, showing each scheme’s accuracy improvement over Baseline. The results reveal that both *UpC-R* and *F-RoT* performs better than Baseline in most cases, showing each component’s own effectiveness. In addition, *UpC-R* always slightly outperforms *F-RoT*, meaning that hybrid pseudo label contributes more to performance improvement than data diversity. More importantly, UpCycling significantly improves accuracy over both ablated versions, verifying that combining hybrid pseudo label and feature augmentation creates critical synergy. The performance gap between UpCycling and the ablated schemes becomes larger as the ratio of labeled data decreases.

Table 3 performs the same comparison in the domain adaptation scenario described in Section 4.2, showing each scheme’s AP_{3D} performance and its relative position between Baseline (0) and Oracle (100). The results show that all the observations in Figure 3 still hold in the domain adaptation scenario. Overall, our results suggest that (1) the effect of hybrid pseudo labels, (2) that of feature augmentation, and (3) the synergistic effect when combining the two components all generally occur regardless of the model, task, and dataset.

Effect of augmentation schemes. We investigate feature augmentation more deeply by evaluating the superiority of *F-GT* and *F-RoT* to other augmentation schemes. To this end, we select three comparison schemes, **Flip**, **RS**, and **Noise**. Flip and RS are used in the SOTA SSL methods on 3D object detection to augment raw-level 3D scenes [38, 44]. For feature-level Flip, we place feature information to its symmetric position on the feature map. For feature-level RS, we nullify randomly selected 5% of feature data. Combination of feature-level Flip and RS is the same as F-3DIoUMatch in Figure 1. Lastly, Noise is an existing feature augmentation method that adds Gaussian noise, which is used for domain generalization of image classification [18].

Table 4 evaluates the augmentation methods in the partial-label scenario described in Section 4.3, showing each scheme’s performance margin compared to Baseline. Interestingly, Flip significantly underperforms Baseline, verifying that feature-level Flip damages important information in 3D scenes. Both Noise and RS have marginal impact on performance, showing that these perturbation strategies do not result in meaningful data diversity. Combining Flip and RS (*i.e.*, F-3DIoUMatch) still performs worse than Baseline due to the negative effect of Flip, which explains why naïve application of SOTA SSL methods at a feature level does not work. In contrast, both *F-GT* and *F-RoT* show their own performance gain and combining the two (*i.e.*, UpCycling) boosts accuracy much more.

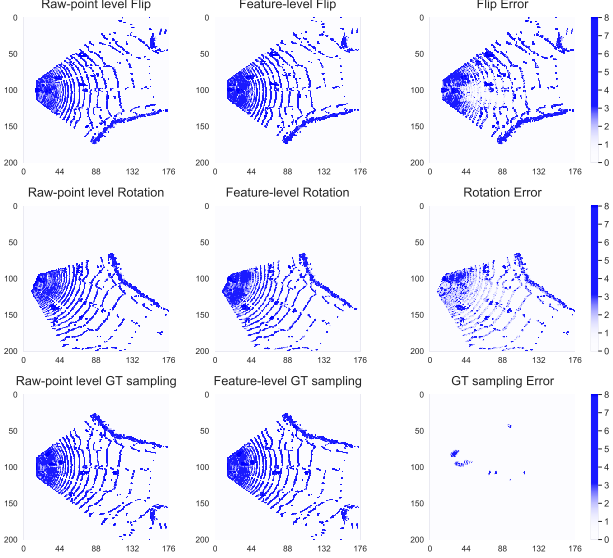


Figure 4. Feature-level scenes for three data augmentation methods: Flip (1st row), Rotation (2nd row), and GT sampling (3rd row). Feature-level scenes of raw-point level augmentation are on the left. Feature-level scenes of feature-level augmentation are in the middle. Heatmaps of RMSE based on comparison between raw-level and feature-level augmentation scenes are on the right.

4.5. Demystifying 3D Scene Feature Augmentation

In this section, we take a deeper look into subtle feature-level 3D scene augmentation. Specifically, we focus on (1) why widely-used Flip damages important information when applied at a feature level and (2) why *F-GT* and *F-RoT* are proper for weak and strong augmentations, respectively.

To this end, Figure 4 depicts activation heat maps of the Bird-eye View (BEV) compression module in SECOND-IoU when Flip, Rotation, and GT sampling are applied to an example 3D scene covering x, y, z axis range 70.4, 80, 4 meters. The figure shows that in the cases of Flip and Rotation, raw-level augmentation (*i.e.*, flipping/rotating the whole point cloud) and feature-level augmentation (*i.e.*, flipping/rotating the feature vector) result in significantly different activations. In both cases, although the two activation heat maps look similar at a glance, taking the difference between the two causes errors that are widely spread over the entire feature map. In contrast, when using GT sampling, raw- and feature-level augmentations provide similar activation heat maps. Although some errors exist, they are placed in restricted areas where GT samples are inserted, which makes GT sampling appropriate for weak augmentation.

Figure 5 provides a visual illustration of why we select Rotation instead of Flip for strong augmentation. If a point cloud is voxelized with each voxel producing its feature value, flipping/rotating the feature vector is similar to flipping/rotating voxels. This means that point locations are shifted not individually but in groups, and the geometric

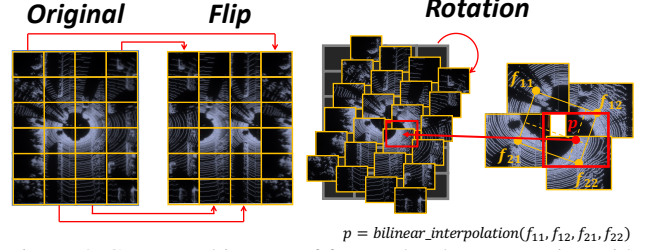


Figure 5. Conceptual images of feature-level augmentation with Flip and Rotation.

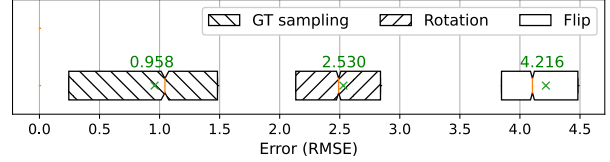


Figure 6. RMSE between raw- and feature-level augmentations of the entire KITTI training dataset. Box range covers the first quartile to the third quartile and the mark ‘x’ indicates the mean value.

relationship between intra-voxel points is maintained; they are neither flipped nor rotated. In the worst case, the group (voxel)-wise flipping causes a valid car object to break apart, making its label detrimental to training. Breaking the geometric relationship between points on the background can also cause severe misinterpretation. In contrast, the group-wise rotation incurs relatively mild perturbation and its bilinear interpolation compensates for the errors, which is more proper for strong augmentation.

Figure 6 confirms our description by showing the average of root mean square error (RMSE) between raw- and feature-level augmentations in the KITTI dataset. While feature-level Flip severely damages original scenes, *F-RoT* significantly reduces errors and *F-GT* causes only marginal errors.

5. Conclusion

In this paper, we have presented UpCycling, a novel semi-supervised learning framework for 3D object detection models that does not utilize unlabeled raw-level 3D scenes but only de-identified intermediate features. To the best of our knowledge, UpCycling is the first framework that tackles labeling cost, privacy leakage, and AV-side computation burden altogether. Our deep investigation of feature-based learning reveals that combining *hybrid pseudo label*, *F-GT*, and *F-RoT* significantly improves pseudo-label quality and data diversity. Results from various experiments demonstrate that UpCycling achieves SOTA accuracy with large margins in both partial-label and domain adaptation scenarios, regardless of the model, dataset, and task (difficulty setting or average precision of BEV/3D view). With the superior performance, UpCycling discloses the value of unlabeled feature-based learning in the context of 3D object detection, in terms of both privacy and accuracy.

Acknowledgement

This work was supported by the National Research Foundation of Korea(NRF) grant funded by the Korea government(MSIT) (No. 2020R1A2C2101815).

References

- [1] bostondiditeam. Exploratory findings for the kitti vision benchmark suite. <https://github.com/bostondiditeam>, 2017. 6
- [2] Feng Cen, Xiaoyu Zhao, Wuzhuang Li, and Guanghui Wang. Deep feature augmentation for occluded image classification. *Pattern Recognition*, 111:107737, 2021. 2
- [3] Peng Chu, Xiao Bian, Shaopeng Liu, and Haibin Ling. Feature space augmentation for long-tailed data. In *European Conference on Computer Vision*, pages 694–710. Springer, 2020. 2
- [4] Ekin D Cubuk, Barret Zoph, Jonathon Shlens, and Quoc V Le. Randaugment: Practical automated data augmentation with a reduced search space. In *Proceedings of the IEEE/CVF Conference on Computer Vision and Pattern Recognition Workshops*, pages 702–703, 2020. 2
- [5] Jiajun Deng, Shaoshuai Shi, Peiwei Li, W. Zhou, Yanyong Zhang, and H. Li. Voxel r-cnn: Towards high performance voxel-based 3d object detection. In *AAAI*, 2021. 2, 4
- [6] Terrance DeVries and Graham W Taylor. Improved regularization of convolutional neural networks with cutout. *arXiv preprint arXiv:1708.04552*, 2017. 2
- [7] David Eckhoff and Christoph Sommer. Driving for big data? privacy concerns in vehicular networking. *Security & Privacy, IEEE*, 12:77–79, 01 2014. 1
- [8] Andreas Geiger, Philip Lenz, and Raquel Urtasun. Are we ready for autonomous driving? the kitti vision benchmark suite. In *Conference on Computer Vision and Pattern Recognition (CVPR)*, 2012. 1, 2, 5
- [9] Otkrist Gupta and Ramesh Raskar. Distributed learning of deep neural network over multiple agents. *Journal of Network and Computer Applications*, 116:1–8, 2018. 1, 2, 3
- [10] Martin Hahner, Dengxin Dai, Alexander Liniger, and Luc Van Gool. Quantifying data augmentation for lidar based 3d object detection. *arXiv preprint arXiv:2004.01643*, 2020. 4
- [11] John Houston, Guido Zuidhof, Luca Bergamini, Yawei Ye, Ashesh Jain, Sammy Omari, Vladimir Iglovikov, and Peter Ondruska. One thousand and one hours: Self-driving motion prediction dataset. *CoRR*, abs/2006.14480, 2020. 1, 2, 5
- [12] Jisoo Jeong, Seungeui Lee, Jeessoo Kim, and Nojun Kwak. Consistency-based semi-supervised learning for object detection. In H. Wallach, H. Larochelle, A. Beygelzimer, F. d'Alché-Buc, E. Fox, and R. Garnett, editors, *Advances in Neural Information Processing Systems 32*, pages 10759–10768. Curran Associates, Inc., 2019. 2
- [13] Jakub Konečný, H. Brendan McMahan, Felix X. Yu, Peter Richtárik, Ananda Theertha Suresh, and Dave Bacon. Federated learning: Strategies for improving communication efficiency, 2016. 1, 2
- [14] Varun Kumar, Hadrien Glaude, Cyprien de Lichy, and William Campbell. A closer look at feature space data augmentation for few-shot intent classification. *arXiv preprint arXiv:1910.04176*, 2019. 2
- [15] Samuli Laine and Timo Aila. Temporal ensembling for semi-supervised learning, 2016. 2
- [16] A. H. Lang, S. Vora, H. Caesar, L. Zhou, J. Yang, and O. Beijbom. Pointpillars: Fast encoders for object detection from point clouds. In *2019 IEEE/CVF Conference on Computer Vision and Pattern Recognition (CVPR)*, pages 12689–12697, June 2019. 2, 3, 4
- [17] Dong-Hyun Lee. Pseudo-label : The simple and efficient semi-supervised learning method for deep neural networks. *ICML 2013 Workshop : Challenges in Representation Learning (WREPL)*, 07 2013. 2
- [18] Pan Li, Da Li, Wei Li, Shaogang Gong, Yanwei Fu, and Timothy M Hospedales. A simple feature augmentation for domain generalization. In *Proceedings of the IEEE/CVF International Conference on Computer Vision*, pages 8886–8895, 2021. 2, 7
- [19] Bo Liu, Xudong Wang, Mandar Dixit, Roland Kwitt, and Nuno Vasconcelos. Feature space transfer for data augmentation. In *Proceedings of the IEEE Conference on Computer Vision and Pattern Recognition (CVPR)*, June 2018. 2
- [20] Brendan McMahan, Eider Moore, Daniel Ramage, Seth Hampson, and Blaise Agüera y Arcas. Communication-Efficient Learning of Deep Networks from Decentralized Data. In Aarti Singh and Jerry Zhu, editors, *Proceedings of the 20th International Conference on Artificial Intelligence and Statistics*, volume 54 of *Proceedings of Machine Learning Research*, pages 1273–1282, Fort Lauderdale, FL, USA, 20–22 Apr 2017. PMLR. 3
- [21] Yang Ming and Xiaopeng Yu. Efficient privacy-preserving data sharing for fog-assisted vehicular sensor networks. *Sensors*, 20(2), 2020. 1
- [22] T. Miyato, S. Maeda, M. Koyama, and S. Ishii. Virtual adversarial training: A regularization method for supervised and semi-supervised learning. *IEEE Transactions on Pattern Analysis and Machine Intelligence*, 41(8):1979–1993, 2019. 2
- [23] Charles R Qi, Hao Su, Kaichun Mo, and Leonidas J Guibas. Pointnet: Deep learning on point sets for 3d classification and segmentation. In *Proceedings of the IEEE conference on computer vision and pattern recognition*, pages 652–660, 2017. 3
- [24] Charles Ruizhongtai Qi, Li Yi, Hao Su, and Leonidas J Guibas. Pointnet++: Deep hierarchical feature learning on point sets in a metric space. *Advances in neural information processing systems*, 30, 2017. 3
- [25] Sashank Reddi, Zachary Charles, Manzil Zaheer, Zachary Garrett, Keith Rush, Jakub Konečný, Sanjiv Kumar, and H Brendan McMahan. Adaptive federated optimization. *arXiv preprint arXiv:2003.00295*, 2020. 3
- [26] Amirhossein Reisizadeh, Aryan Mokhtari, Hamed Hassani, Ali Jadbabaie, and Ramtin Pedarsani. Fedpaq: A communication-efficient federated learning method with periodic averaging and quantization. In Silvia Chiappa and

- Roberto Calandra, editors, *Proceedings of the Twenty Third International Conference on Artificial Intelligence and Statistics*, volume 108 of *Proceedings of Machine Learning Research*, pages 2021–2031. PMLR, 26–28 Aug 2020. **1**
- [27] Shaoshuai Shi, Chaoxu Guo, Li Jiang, Zhe Wang, Jianping Shi, Xiaogang Wang, and Hongsheng Li. Pv-rcnn: Point-voxel feature set abstraction for 3d object detection. In *Proceedings of the IEEE/CVF Conference on Computer Vision and Pattern Recognition (CVPR)*, June 2020. **2, 3, 4**
- [28] Shaoshuai Shi, Xiaogang Wang, and Hongsheng Li. Pointrcnn: 3d object proposal generation and detection from point cloud. In *The IEEE Conference on Computer Vision and Pattern Recognition (CVPR)*, June 2019. **3**
- [29] Nir Shlezinger, Mingzhe Chen, Yonina C. Eldar, H. Vincent Poor, and Shuguang Cui. Uveqfed: Universal vector quantization for federated learning. *IEEE Transactions on Signal Processing*, 69:500–514, 2021. **1**
- [30] Abhishek Singh, Praneeth Vepakomma, Otkrist Gupta, and Ramesh Raskar. Detailed comparison of communication efficiency of split learning and federated learning. *arXiv preprint arXiv:1909.09145*, 2019. **1, 3**
- [31] Kihyuk Sohn, David Berthelot, Chun-Liang Li, Zizhao Zhang, Nicholas Carlini, Ekin D. Cubuk, Alex Kurakin, Han Zhang, and Colin Raffel. Fixmatch: Simplifying semi-supervised learning with consistency and confidence. *arXiv preprint arXiv:2001.07685*, 2020. **2**
- [32] Pei Sun, Henrik Kretschmar, Xerxes Dotiwalla, Aurelien Chouard, Vijaysai Patnaik, Paul Tsui, James Guo, Yin Zhou, Yuning Chai, Benjamin Caine, Vijay Vasudevan, Wei Han, Jiquan Ngiam, Hang Zhao, Aleksei Timofeev, Scott Etinger, Maxim Krivokon, Amy Gao, Aditya Joshi, Yu Zhang, Jonathon Shlens, Zhifeng Chen, and Dragomir Anguelov. Scalability in perception for autonomous driving: Waymo open dataset. In *Proceedings of the IEEE/CVF Conference on Computer Vision and Pattern Recognition (CVPR)*, June 2020. **1, 2, 5**
- [33] Antti Tarvainen and Harri Valpola. Mean teachers are better role models: Weight-averaged consistency targets improve semi-supervised deep learning results, 2017. **2, 4**
- [34] OpenPCDet Development Team. Openpcdet: An open-source toolbox for 3d object detection from point clouds. <https://github.com/open-mmlab/OpenPCDet>, 2020. **2, 3**
- [35] Praneeth Vepakomma, Otkrist Gupta, Tristan Swedish, and Ramesh Raskar. Split learning for health: Distributed deep learning without sharing raw patient data. *arXiv preprint arXiv:1812.00564*, 2018. **1, 3**
- [36] Praneeth Vepakomma, Tristan Swedish, Ramesh Raskar, Otkrist Gupta, and Abhimanyu Dubey. No peek: A survey of private distributed deep learning. *arXiv preprint arXiv:1812.03288*, 2018. **2**
- [37] Vikas Verma, Alex Lamb, Christopher Beckham, Amir Najafi, Ioannis Mitliagkas, David Lopez-Paz, and Yoshua Bengio. Manifold mixup: Better representations by interpolating hidden states. In Kamalika Chaudhuri and Ruslan Salakhutdinov, editors, *Proceedings of the 36th International Conference on Machine Learning*, volume 97 of *Proceedings of Machine Learning Research*, pages 6438–6447. PMLR, 09–15 Jun 2019. **2**
- [38] He Wang, Yezhen Cong, Or Litany, Yue Gao, and Leonidas J Guibas. 3dioumatch: Leveraging iou prediction for semi-supervised 3d object detection. In *Proceedings of the IEEE/CVF Conference on Computer Vision and Pattern Recognition*, pages 14615–14624, 2021. **1, 2, 4, 6, 7**
- [39] Hongyi Wang, Mikhail Yurochkin, Yuekai Sun, Dimitris Papailiopoulos, and Yasaman Khazaeni. Federated learning with matched averaging. *arXiv preprint arXiv:2002.06440*, 2020. **3**
- [40] Yan Wang, Xiangyu Chen, Yurong You, Li Erran Li, Bharath Hariharan, Mark Campbell, Kilian Q Weinberger, and Wei-Lun Chao. Train in germany, test in the usa: Making 3d object detectors generalize. In *Proceedings of the IEEE/CVF Conference on Computer Vision and Pattern Recognition*, pages 11713–11723, 2020. **5, 6**
- [41] Jinbo Xiong, Renwan Bi, Mingfeng Zhao, Jingda Guo, and Qing Yang. Edge-assisted privacy-preserving raw data sharing framework for connected autonomous vehicles. *IEEE Wireless Communications*, 27(3):24–30, 2020. **1**
- [42] Yan Yan, Yuxing Mao, and Bo Li. Second: Sparsely embedded convolutional detection. *Sensors*, 18(10):3337, Oct 2018. **2, 3, 4**
- [43] Jihan Yang, Shaoshuai Shi, Zhe Wang, Hongsheng Li, and Xiaojuan Qi. St3d: Self-training for unsupervised domain adaptation on 3d object detection. In *Proceedings of the IEEE/CVF Conference on Computer Vision and Pattern Recognition*, pages 10368–10378, 2021. **2, 6**
- [44] Na Zhao, Tat-Seng Chua, and Gim Hee Lee. Sess: Self-ensembling semi-supervised 3d object detection. In *Proceedings of the IEEE/CVF Conference on Computer Vision and Pattern Recognition*, pages 11079–11087, 2020. **1, 2, 4, 7**
- [45] Yin Zhou and Oncel Tuzel. Voxelnet: End-to-end learning for point cloud based 3d object detection. In *2018 IEEE/CVF Conference on Computer Vision and Pattern Recognition*, pages 4490–4499, 2018. **2, 3, 4**